Kinetics of HOBr Uptake on NaBr and NaCl Surfaces at Varying Relative Humidity

Liang T. Chu,* Guowang Diao, and Liang Chu†

Wadsworth Center, NYS Department of Health and State University of New York, P.O. Box 509, Albany, New York 12201-0509

Received: September 20, 2001; In Final Form: April 1, 2002

The uptake kinetics of HOBr on NaBr and NaCl particle-film surfaces has been studied in a flow reactor coupled with a differentially pumped quadrupole mass spectrometer. Spray-deposited and aerosol-deposited salt-particle films were used for the measurement of HOBr reactivity. A rapid gas−surface reaction was observed on the NaBr surface at 250 K, and the initial uptake coefficient γ_w was determined to be 0.029 ± 0.004 and 0.021 ± 0.004 at relative humidities (RH) of 0.5 and 12.2%, respectively. γ_w is lower at 260 K. For the reaction on NaCl particle surfaces, γ_w decreases slightly from $2.0 \pm 0.3 \times 10^{-3}$ to $8.1 \pm 1.3 \times 10^{-4}$ at 250 K as RH increases from 1.5 to 18.2%. The results are interpreted in terms of the mechanism HOBr(ad) + NaX(s) → BrX + NaOH(s), which involves the adsorption of HOBr on the surface, with the reactions occurring mainly on a NaX surface domain without water coverage at low RH. The surface morphology of the particle films was characterized by scanning electron microscopy, and the tortuosity factor, τ, of the NaCl particle film was determined to be 2.18. γ_w was corrected for internal surface effects to provide "true" uptake coefficients γ_t. Typical γ_t values for HOBr on NaBr and NaCl at 250 K and RH of 10% are 2.5×10^{-3} and 5×10^{-5}, respectively. Calculations suggest that the HOBr heterogeneous activation on NaBr may be competitive, if surface regeneration occurs.

I. Introduction

The dramatic loss of surface-layer ozone at sunrise has been observed in the high Arctic over the past decade.[1] High levels of BrO (20−30 pptv) were found in the polar boundary layer, and these events were always associated with the ozone loss. The observation is still only partly explained in terms of halogen chemistry, and the details are not completely understood.[2−5] More recently, even higher levels of BrO (mixing ratio ∼86 pptv) were reported from the Dead Sea basin, where complete boundary-layer ozone destruction was associated with episodes of high BrO.[6] It is believed that Br species are activated via heterogeneous processes and play a critical role in the boundary-layer ozone destruction. Barrie et al. have suggested an ozone-loss mechanism involving catalytic Br cycles.[1] Br and Cl in sea-salt aerosols were proposed to be potential sources for the generation of photochemically active halogen species.[7]

The activation of Br or Cl by reactions with nitrogen oxides over sea salt (mainly NaCl and NaBr) has been extensively studied.[8−15]

$$N_2O_5 + NaCl(s) \rightarrow ClNO_2 + NaNO_3(s) \qquad (1)$$

The activation of Br and Cl on sea-salt particles also extends to reactions with Cl and Br reservoir compounds such as $ClONO_2$ and HOBr with NaCl and KBr.[16−21] The latter was suggested to play a role in the generation of active Br.[22,23] Abbatt and Waschewsky showed that the uptake coefficient, γ, of HOBr over deliquescent NaCl aerosols depended on the aerosol acidity.[21] γ decreased from 0.2 for buffered aerosols to $<1.5 \times 10^{-3}$ for unbuffered aerosols at [HOBr] = 10^{12}−10^{13} molecules/cm^3. Mochida et al. showed that the initial uptake coefficient of HOBr on NaCl powder was approximately 9×10^{-4} at [HOBr] = 1×10^{11} molecules/cm^3.[18] If we compare the uptake coefficient of HOBr on NaCl powder with that on the deliquescent NaCl aerosol, it suggests that the uptake coefficient likely depends on water content. On the other hand, studies have shown that both the water vapor and adsorbed water had an impact on the uptake of HNO_3 on NaCl surfaces.[11,12,24] Davids and Cox showed that the uptake coefficient γ of HNO_3 on NaCl increases with increasing relatively humidity (RH) (0−35%).[11] They suggested that the observation was closely associated with the adsorption of water on NaCl surfaces.[25−27]

The uptake coefficient of N_2O_5 on $(NH_4)_2SO_4$ aerosols decreases from 0.05 to 0.017 as RH increases from 50% to 93.5% at 297 K.[28] The uptake coefficient of N_2O_5 on sulfuric acid aerosols decreases from 0.05 to 0.02 as RH increases from 0.7 to 80%.[28−30] The hydrolysis of N_2O_5 on aerosols is expected to be dependent on RH. However, the most intriguing aspect of the result is that γ *decreases* slightly as RH increases. This implies that water may not play a direct reactive role in the rate-determining step of the hydrolysis reaction.[28] Behnke et al. found that the reaction of N_2O_5 on wet NaCl aerosols had two different reaction pathways.[31] One involves the hydrolysis of N_2O_5, and the other is the formation of $ClNO_2$. The $ClNO_2$ yield was higher at a low RH.[32] The experimental evidence leads us to hypothesize that the uptake of HOBr on NaX may depend either on the amount of water on the NaX surface or on the RH.

Under typical atmospheric conditions, atmospheric aerosols are surrounded by water vapor. The physiochemical properties of the aerosols are a function of water content.[33] The effect of RH on the uptake of HOBr on NaCl and NaBr was not previously investigated. This fact motivated us to investigate the heterogeneous reactions of HOBr on NaBr and NaCl aerosol

* To whom correspondence should be addressed. E-mail: lchu@albany.edu.
† Current address: University of California, 1 Shields Ave., Davis, CA 95616-8627.

10.1021/jp013594g CCC: $22.00
Published on Web 05/09/2002

particle surfaces as a function of RH and temperature. Our study sheds light on the mechanism of Br and Cl activation on sea-salt particle surfaces as well as on the role of adsorbed water in these reactions. It also provides uptake coefficients as a function of RH.

We report heterogeneous uptake of HOBr on both NaBr and NaCl surfaces via the two following reactions:

$$HOBr + NaBr \rightarrow Br_2 + NaOH \quad (2)$$

$$HOBr + NaCl \rightarrow BrCl + NaOH \quad (3)$$

Our study was carried out in a fast flow reactor, and the loss of HOBr and products was detected by a quadrupole mass spectrometer (QMS). In the following sections, we will briefly describe the experimental procedures. The initial uptake coefficient as a function of RH and temperature for reactions 2 and 3 will be presented. The results were modeled by a gas−surface reaction scheme. The NaX surface morphology was examined using scanning electron microscope (SEM), and the effect of surface porosity on the measured uptake coefficient was studied in detail.

II. Experimental Section

Apparatus. The experiments were conducted in a fast flow reactor coupled to a differentially pumped quadrupole mass spectrometer. The reactor was similar to the one used in previous studies.[34,35] However, several major modifications were made on the flow reactor which are described below. The inner diameter of the Pyrex flow tube was 2.63 cm, and it was 35 cm in length. A detachable cylindrical glass tube with outer diameter of 2.55 cm and inner diameter of 2.20 cm was tightly fitted inside the flow tube. The salt-particle film was prepared on the inner wall of the detachable glass tube. HOBr was admitted via a movable injector positioned at the center of the flow reactor. The movable injector consisted of two concentric tubes; the inner one was a small capillary and was used to admit HOBr to the reactor. The downstream end of the outside tube was sealed to the inner tube. Room-temperature dry air was purged between these two tubes so that HOBr and water vapor would not condense on the wall of the capillary at low temperature. The temperature of the reactor was regulated by a liquid-nitrogen-cooled methanol circulator (Neslab) and was measured with two J-type thermocouples (Omega, DP-41) located in the middle and at the downstream end of the flow tube. The thermocouples were calibrated at the triple point of water (273.2 K) with an accuracy of ±0.2 K. The temperature on the inner-wall surface of the detachable glass tube was measured in a separate experiment using a thin-gauge thermocouple wire under the same experimental conditions. The results showed that the temperature on the inner-wall surface of the detachable glass tube was 0.2−0.3 K warmer than that measured on the flow-tube surface. The temperatures reported in the paper were corrected for this difference. The total pressure in the flow reactor was controlled by a downstream throttle valve (MKS Instrument, Model 651C), and the stability was better than 0.001 Torr. The pressure was measured using a high-precision Baraton gauge (MKS, Model 690A) located at the downstream end of the flow tube. The typical pressure used in this study was either 0.5 or 1.0 Torr.

Preparation of Salt Films. *NaBr Film Preparation*. The detachable glass tube was cleaned with dichromate sulfuric acid cleaning solutions and rinsed several times with distilled water. The tube was then dried in an oven at 160 °C. Saturated NaBr−CH_3OH solutions were sprayed on the inner wall of the tube directly, while the detachable glass tube was heated by a heating tape at 120 °C. NaBr was deposited on the wall surface, while excess CH_3OH evaporated rapidly at the warmer temperature. The NaBr film was then dried in the oven for 1 h at 160 °C. The amount of NaBr deposited was determined by an analytical balance (0.1 mg accuracy). From the bulk density (2.1 g/cm^3; see below for details) and the geometric surface area of the detachable glass tube, the thickness of the film was determined. The typical thickness of the NaBr particle film was 15 ± 2 μm.

NaCl Film Preparation. The solubility of NaCl in methanol is lower than for NaBr, and it is difficult to prepare a uniform, micron-sized NaCl film using the above method. A different approach was used to prepare NaCl particle films. The detachable glass tube was heated by a heating tape and the temperature was kept at approximately 150 °C. The heated tube was mounted in a vertical position. NaCl aerosols were generated by a homemade capillary atomizer from saturated NaCl−water solutions. The size of the atomizer was smaller than the inner diameter of the detachable glass tube. NaCl solutions were pressurized by 1.5-atm N_2 gas to generate micron-sized NaCl−H_2O aerosols through the atomizer. The atomizer was admitted into the vertically mounted detachable glass tube and the aerosols were sprayed on the inner wall of the tube. Water moisture was evaporated rapidly at 150 °C, and NaCl was deposited on the wall surface as micron-sized particles. As the atomizer was slowly pulled downward at a constant speed, a uniform fine NaCl particle film was formed on the glass wall. The thickness of the film was determined by the amount of NaCl deposited on the wall surface, which varied by the deposition time. The detachable glass tube was finally heated in the oven at 150−200 °C for 1 h to ensure that water moisture was evaporated.

The advantage of this method is that both the amount of NaCl deposited on the detachable glass tube surface and the particle size distributions can be controlled. This allowed us to study the effect of particle film morphology on the uptake coefficient. Both NaCl and NaBr particle films were freshly prepared for every experiment.

Measurement of the Bulk Density. The NaX particle film was deposited onto a glass rod (2.8 mm in diameter and 19 cm in length) using the methods described above. The film was dried in the oven, and the mass was determined on the analytical balance. The salt-deposited rod was then protected by an ultrathin layer of an acrylic film. The volume of both the protected salt glass rod and the bare glass rod was measured by the displacement of water in a high-precision 2-ml pipet (precision ±0.005 mL). The volume of the protected salt film was determined. The volume of the protective acrylic film was approximately determined by the difference in volume between the acrylic-protected glass rod and the bare glass rod. This volume was subtracted from the volume of the protected salt film, and the volume of the salt-particle film was thus obtained. The bulk density of the NaBr and NaCl films was determined to be 2.1 ± 0.3 and 1.1 ± 0.2 g·cm^{-3}, respectively.

Preparation and Calibration of HOBr. The HOBr solution was prepared using the method described in our previous work.[36] Briefly, 3.9 g of Ag_2SO_4 (Aldrich, 99%) were dissolved into 100 mL of 0.25 M H_2SO_4 in a glass flask cooled in an ice−water bath. Br_2 (Aldrich, 99.5%) was added to the solution drop by drop, while the solution was stirred, until the orange color of excess Br persisted. After the solution settled in the glass flask, the solution was decanted into a separatory funnel. Carbon tetrachloride was used to extract the excess Br_2 in the solution,

and the heavier CCl_4 phase was removed from the funnel. A slightly yellowish-clear HOBr solution was obtained and was kept in a bubbler in the dark at 273.2 K.

HOBr vapor was bubbled into the movable injector using He carrier gas. FEP tubing and Teflon Swagelok fittings were used. The flow of HOBr was controlled by Halocarbon grease-treated stainless-steel needle valve. The flow rate of the HOBr and He mixture was measured by a mass flow meter (Hasting−Teledyne), which was corrected for the water vapor. The typical flow rate of the mixture was 10 sccm. Additional He was mixed with the HOBr flow at the inlets of the injector to minimize loss of HOBr. All flow rates were controlled by either the mass flow controller or metering valves. The transfer lines were first passivated by flowing HOBr until a stable signal was reached as monitored by QMS.

Impurities in the HOBr−He mixture stream were monitored by QMS. We found that Br_2 ($m/e = 180$) was the major impurity. Other QMS signals at $m/e = 196$ (Br_2O) and 80 were small (<10%). The signal at $m/e = 80$ could be HBr. In a separate experiment, we monitored the loss of HBr ($P_{HBr} \sim 10^{-6}$ Torr) onto the dry salt surface at room temperature and did not find any measurable loss. When there was water vapor ($\sim 10^{-3}$ Torr) in transfer lines, HBr was lost on the lines. This suggests that the HBr impurity, if any, should not affect the HOBr uptake measurements. Gas-phase Br_2 was from the HOBr solution and from the decomposition of the HOBr vapor. The following procedures were used to minimize Br_2. Br_2 accumulated during the night in the HOBr bubbler was purged by He prior to experiments. The needle valve, which controlled the flow of HOBr, was cleaned frequently and was treated with Halocarbon grease to minimize decomposition of HOBr on metal surfaces. Both HOBr and Br_2 signals were monitored using QMS until their signal levels were stable prior to every uptake measurement. The Br_2 signal intensity was usually less than that of HOBr (5−50%).

The [HOBr] was calibrated using the following experiment.[36] An ice film was prepared on the wall of the flow tube at 190 K (without the detachable glass tube). A higher [HOBr] ($\sim 5 \times 10^{-6}$ Torr) was exposed to the ice surface for more than 30 min so that the surface was nearly saturated. A lower [HCl] ($\sim 5 \times 10^{-7}$ Torr) was allowed to react with the adsorbed HOBr to produce BrCl. The BrCl signal was monitored by QMS at $m/e^- = 114$. The number of BrCl molecules formed was equal to that of HCl. The BrCl sensitivity for the QMS (count/Torr sec) was determined. Subsequently, we reversed the ratio of [HOBr] to [HCl]. We determined the signal ratio of HOBr to BrCl, and thus the HOBr sensitivity was determined.

The sensitivity of the QMS may change slightly over a period of weeks. We also determined the signal ratio of HOBr to H_2O over the HOBr solution. Since HOBr solutions were very dilute, the water vapor pressure over the solutions was approximately constant at 273 K. The [HOBr]/[H_2O] signal ratio provided an excellent guideline to maintain constant [HOBr] throughout the entire experiment.

Relative Humidity. Water vapor, carried by He from a temperature-controlled water bubbler, was admitted to the flow reactor to control the RH over NaX surfaces, and the water vapor was allowed to flow a sufficiently long time to achieve an equilibrium with the surface. The flow rate of water−He mixture was controlled by a metering valve and measured by the mass flow meter (Hasting−Teledyne). A low flow rate (<100 sccm) was chosen to ensure the equilibrium between water and its vapor in the bubbler and to maintain a constant water vapor-to-He mixing ratio. The water bubbler was kept at 278 K to minimize the loss of water vapor onto the FEP transfer line, which was at room temperature. In a separate experiment, QMS was used to monitor the water vapor signal at various water flow rates. We found that the water signal varied linearly with the flow rates of the water−He stream, suggesting that the water vapor was in equilibrium with its liquid in the water bubbler and the water/He mixing ratio was equal to their partial pressure ratio. The total water vapor in the reactor was the sum of the water vapor from both the water vapor−He mixture and the water vapor in HOBr. The water vapor pressure in the HOBr solution was approximately equal to saturation water vapor pressure at 273 K. The water vapor pressure in the reactor could be estimated from the flow rates and mixing ratios. However, error was introduced at lower RH where the flow rate of the water−He mixture was comparable with the HOBr flow rate (10 sccm). To eliminate the error, the water vapor pressure was calibrated against the ice vapor pressure at 203−218 K ($P_{ice} = 1.94 \times 10^{-3}$ Torr at 203 K[37]) using the QMS under the same total pressure and flow conditions. The estimated water vapor pressure in the reactor was within 8% of the vapor pressure measured by QMS. In this paper, the reported RH was measured by QMS and the relative error was estimated to be <8%.

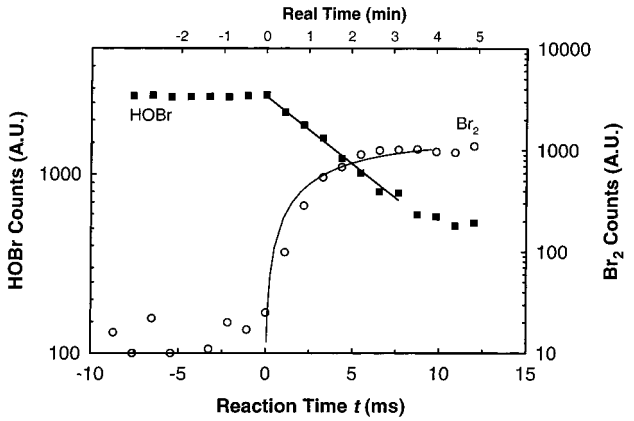

Figure 1. Uptake of HOBr on a NaBr particle film surface. A plot of log [HOBr] versus reaction time t showed that the pseudo-first-order rate k_s was 186 s^{-1} and $\gamma_w = 0.022$ at 250.3 K and $P_{HOBr} = 1.1 \times 10^{-6}$ Torr. The formation of Br_2 was observed, and the rate constant was determined to be 194 s^{-1}. The real time is shown on the top axis. See text for details.

Measurement of the Uptake Coefficient. The uptake coefficient of HOBr on salt-particle films was measured by monitoring the gas-phase HOBr loss over the salt surface. Before the measurement, the injector was placed in front of the salt-particle film (the downstream end of the flow reactor), and the initial HOBr signal was recorded by QMS at $m/e = 96$. The injector was pulled back over the salt surface 2 cm at a time. The loss of HOBr was recorded as a function of the injector position, z. The typical data-acquisition time for each point was 10 s. The decay of gas-phase HOBr on the salt surface can be described as[35,38]

$$\ln[\mathrm{HOBr}]_z = -k_s(z/v) + \ln[\mathrm{HOBr}]_0 \qquad (4)$$

where $[HOBr]_z$ and $[HOBr]_0$ are the concentrations of gas-phase HOBr when the injector is at position z and that at the reference point 0, respectively, v is the mean flow velocity, and k_s is the pseudo-first-order loss rate constant. k_s was determined by a plot of $\ln[HOBr]_z$ versus the reaction time $t = z/v$. A typical experimental result for the HOBr loss on a NaBr film surface is shown in Figure 1. k_s was determined to be 186 s^{-1} using the data collected at $t < 8$ ms. After the gas-phase axial and

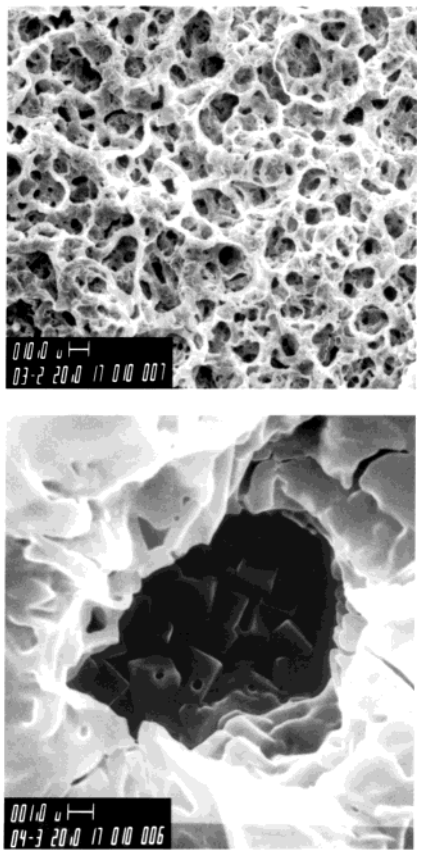

Figure 2. Scanning electron micrographs of NaCl particle films as prepared by depositing NaCl−H_2O aerosols on a glass surface. (Top) NaCl film is porous; (bottom) salt granules can be treated approximately by a layered structure. A relationship between the film thickness and number of granule layers N_L can be determined from this micrograph. Scale bars are in 10.0 μm (top) and 1.0 μm (bottom), respectively.

radial diffusion correction was applied using a standard method,[39] the corrected rate constant, k_w, was determined to be 232 s^{-1}. The diffusion coefficient of HOBr in He and water vapor was calculated using[40]

$$D_{HOBr} = \left(\frac{x_{He}}{D^{HOBr}_{He}} + \frac{x_{water}}{D^{HOBr}_{Water}} \right)^{-1} \quad (5)$$

where x_{He} and x_{water} are the mole fractions of He and water, respectively. D^{HOBr}_{He} and D^{HOBr}_{water} are the diffusion coefficients of HOBr in helium and water, respectively; they were estimated to be 0.340 and 0.121 $cm^2 \cdot s^{-1}$ at 250 K.[36,40] The uptake coefficient, γ, was calculated by[38]

$$\gamma = 2rk_w/(\omega + rk_w) \quad (6)$$

where r is the radius of the detachable glass tube (1.10 cm), and ω is the mean molecular velocity for HOBr at 250 K. When the HOBr uptake was measured on a freshly prepared clean salt surface, we called the uptake coefficient to be the initial uptake coefficient, γ_w.

The surface morphology of salt-particle films was examined using both the optical microscope and SEM. The NaCl particle films appeared "uniform" under a low-magnification optical microscope; however, the fine salt-particle films used in this study appeared porous under SEM in Figure 2. We adopted a pore-diffusion model to correct for the internal surface areas of the particle film[41,42] The model has been successfully applied to treat sea salt and metal oxides.[10,43] The bulk densities ρ_b of

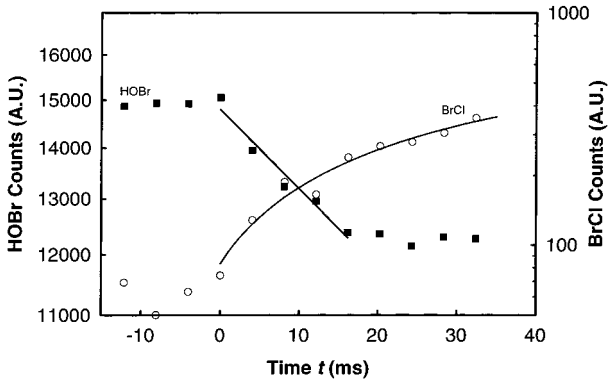

Figure 3. HOBr uptake on an aerosol-deposited fine NaCl particle surface. A plot of log [HOBr] vs t showed k_s to be 12.4 s^{-1} and $\gamma_w = 1.2 \times 10^{-3}$ at 250.7 K. The formation of BrCl was detected by QMS at $m/e = 114$ and is shown on the right-hand axis of the plot. The rate constant k_s was determined to be 13.5 s^{-1}.

NaBr and NaCl films were measured to be 2.1 and 1.1 $g \cdot cm^{-3}$, respectively. The true densities ρ_t of NaBr and NaCl are 3.20 and 2.17 $g \cdot cm^{-3}$,[37] respectively. The ratio of ρ_b/ρ_t for NaBr is 0.66, which is close to 0.74, a value predicted by the pore-diffusion model on the basis of the hexagonal close packing (HCP) of spheres.[42] The density ratio for NaCl is 0.51, which almost coincides with the value of 0.52 predicted by simple cubic packing (SCP).[42] The experimental data were treated using two different granule-packing structures.

The "true" uptake coefficient, γ_t, can be calculated by eqs 7 and 8 for SCP and HCP,[42] respectively:

$$\gamma_t = \frac{\gamma_w}{(\pi/2)[1 + \eta(2N_L - 1)]} \quad (7)$$

$$\gamma_t = \frac{\sqrt{3}\gamma_w}{\pi\{1 + \eta[2(N_L - 1) + (3/2)^{1/2}]\}} \quad (8)$$

where η is the effectiveness factor defined by the fraction of the film surface that participates in the reaction. Its determination will be given in the Results section. N_L is the number of granule layers, which was determined by SEM.

Results

Uptake of HOBr on NaCl. Figure 3 shows the loss of HOBr on a NaCl aerosol-deposited particle film at 250.7 K. The gas-phase HOBr signal decreased with time t over the NaCl surface. At the same time, the formation of BrCl was observed. A plot of the BrCl signal versus t is shown on the right-hand axis of Figure 3. The BrCl signal was undetectable by the QMS without the presence of the NaCl sample in the flow reactor. This suggests that reaction 3 was occurring on the NaCl surface. An average [BrCl]/[HOBr] ratio was determined to be 0.62 ± 0.39 on the basis of a calibration of the BrCl/HOBr signal ratio from the reaction of HOBr + HCl(s) → BrCl + H_2O(s). A linear plot of log [HOBr] versus t suggests the loss of HOBr on the NaCl surface be to pseudo-first-order. The pseudo-first-order wall-loss rate constant was determined to be $k_s = 12.4$ s^{-1}. After the gas-phase diffusion corrections were taken into consideration, k_w and the initial uptake coefficient γ_w were determined to be 12.8 s^{-1} and 1.2×10^{-3}, respectively. A rate constant k_s was also determined from the formation of BrCl. The BrCl data

TABLE 1: Uptake of HOBr on NaCl Films at 250 K[a]

RH%	T (K)	v (m·s^{-1})	k_s (s^{-1})	k_w (s^{-1})	γ_w	γ_t[b]
1.5 ± 0.2	250.1 ± 0.2	4.8	20.5 ± 2.5	21.5 ± 2.2	(2.0 ± 0.3) × 10^{-3}	6.6 × 10^{-5}
1.9 ± 0.2	250.5 ± 0.4	4.9	15.5 ± 2.5	16.0 ± 2.7	(1.5 ± 0.3) × 10^{-3}	4.9 × 10^{-5}
4.6 ± 0.4	250.4 ± 0.2	4.7	15.8 ± 6.0	16.4 ± 6.5	(1.5 ± 0.6) × 10^{-3}	5.0 × 10^{-5}
5.3 ± 0.5	250.1 ± 0.2	4.3	12.3 ± 1.3	12.7 ± 1.4	(1.2 ± 0.2) × 10^{-3}	3.9 × 10^{-5}
6.2 ± 0.6	250.6 ± 0.2	4.8	18.6 ± 2.2	19.4 ± 2.4	(1.8 ± 0.3) × 10^{-3}	6.0 × 10^{-5}
8.3 ± 0.9	249.9 ± 0.3	5.1	12.0 ± 1.4	12.3 ± 1.5	(1.2 ± 0.2) × 10^{-3}	3.9 × 10^{-5}
9.0 ± 1.2	250.3 ± 0.2	4.6	9.3 ± 2.5	9.5 ± 2.6	(8.9 ± 2.5) × 10^{-4}	2.9 × 10^{-5}
9.6 ± 0.8	250.6 ± 0.2	5.6	18.2 ± 7.0	19.0 ± 7.6	(1.8 ± 0.7) × 10^{-3}	5.8 × 10^{-5}
10.7 ± 0.9	250.2 ± 0.2	4.7	11.7 ± 0.7	12.0 ± 0.7	(1.1 ± 0.2) × 10^{-3}	3.6 × 10^{-5}
13.6 ± 1.0	250.6 ± 0.4	4.9	10.9 ± 2.1	11.2 ± 2.2	(1.1 ± 0.2) × 10^{-3}	3.5 × 10^{-5}
14.6 ± 1.1	250.4 ± 0.2	4.9	12.6 ± 1.8	13.0 ± 1.9	(1.2 ± 0.2) × 10^{-3}	3.9 × 10^{-5}
18.2 ± 1.4	250.3 ± 0.2	4.7	8.4 ± 1.1	8.5 ± 1.2	(8.1 ± 1.3) × 10^{-4}	2.6 × 10^{-5}
19.0 ± 1.5	250.4 ± 0.2	4.4	21.5 ± 9.7	22.8 ± 10.8	(2.1 ± 1.0) × 10^{-3}	6.9 × 10^{-5}
19.8 ± 1.4	250.1 ± 0.3	4.4	13.4 ± 1.6	13.9 ± 1.8	(1.3 ± 0.2) × 10^{-3}	4.2 × 10^{-5}
22.5 ± 2.0	250.2 ± 0.3	4.7	22.3 ± 2.9	23.5 ± 3.2	(2.2 ± 0.3) × 10^{-3}	7.2 × 10^{-5}

[a] $P_{HOBr} = (3.8 \pm 0.3) \times 10^{-6}$ Torr, $P_{total} = 1.00$ Torr, thickness = (10.0 ± 0.5) μm. [b] $N_L = 10$ and $\tau = 2.18$ were used in the SCP calculation.

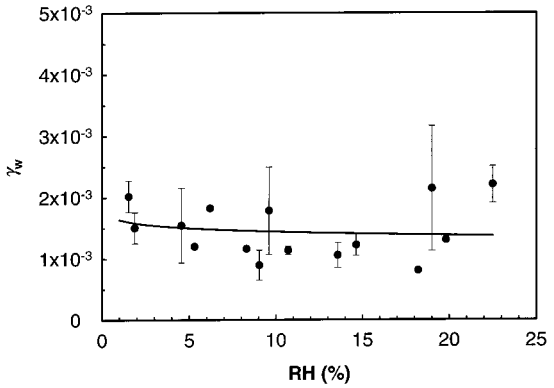

Figure 4. Plot of γ_w as a function of relative humidity (RH) at 250 K for HOBr on aerosol-deposited NaCl particle films. The plot shows that γ_w decreases slightly with RH when RH < 18% and then shows a tendency toward higher γ_w values at RH > 18%. The solid line is a prediction from a kinetic scheme (see text) with a function of $\gamma = a(1 - d\log(bP_{H_2O}))$ where $a = 0.01341$, $b = 0.03078$, and $d = 0.1458$. The error bars represent one standard deviation of the mean.

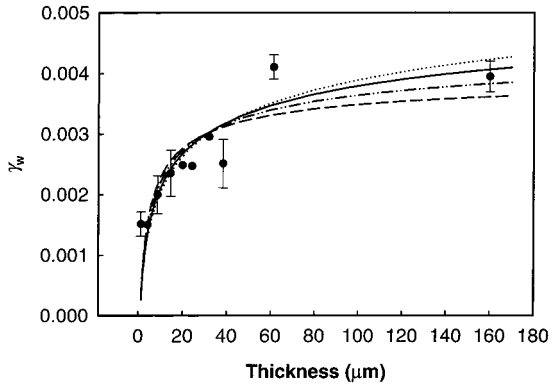

Figure 5. Plot of the initial uptake coefficient as a function of the NaCl film thickness at $P_{HOBr} = 3.2 \times 10^{-6}$ Torr, RH = 1.6%, and 250 K. The solid line was a least-squares fit of the data to the SCP pore-diffusion model (eq 7). γ_t and τ were determined from the least-squares fit to be 6.3×10^{-5} and 2.18, respectively. The dotted, double-dot-dashed, and dashed lines were calculated using the model at $\tau = 1$, 4, and 6, respectively. This suggests that the tortuosity factor τ is not very sensitive to the shape of the curve in the range of $\tau = 1-4$. For illustration purposes, one standard deviation of the mean is included on some data points.

were fitted to $[BrCl] = [BrCl]_\infty(1\text{-}\exp(-k_s t))$, where $[BrCl]_\infty$ is the concentration of BrCl at $t = \infty$. Both k_s and $[BrCl]_\infty$ were fitting parameters. k_s was determined to be 13.5 s^{-1}. This is in good agreement with k_s determined from the HOBr loss.

Figure 4 shows the initial uptake coefficient γ_w as a function of RH. The detailed experimental conditions are listed in Table 1. Each datum except γ_t in the table was the average of two to six determinations. Every determination of k_s was one experiment (e.g., Figure 3) conducted on a freshly prepared NaCl surface. Errors listed in Table 1 are one standard deviation of the mean of a number of determinations. Systematic errors in RH and T were included. The true uptake coefficient, γ_t, was calculated from γ_w using eq 7; the parameters used in the calculation will be discussed below. The uptake coefficient decreases slightly with RH at RH < 18% (Figure 4). When the RH is higher than 18%, the initial uptake coefficient shows a small increase with RH. This observation may be related to the multilayer adsorption of H_2O on NaCl at higher RH (see Discussion).

The initial uptake coefficient γ_w was determined as a function of the thickness, h, of the particle films. The initial uptake coefficient of HOBr rapidly increases with the film thickness when h is less 50 μm, and then γ_w increases gradually up to ~165 μm at 250 K (Figure 5). h is defined as $m/A\rho_b$. This suggests that the particle film is porous and has internal surface areas. HOBr molecules can access internal surfaces by gaseous diffusion from the exterior of the solid. However, at $h > 100$ μm, the diffusion time is longer than the HOBr surface residence time and HOBr molecules cannot effectively access all internal surfaces. This appears as a plateau in Figure 5. On the basis of $\rho_b/\rho_t = 0.51$, the NaCl particle film was modeled by SCP. A nonlinear least-squares fit of all the data, γ_w, to eq 7 is shown as a solid line in Figure 5. η in eq 7 was computed from the following equations[42]

$$\eta = \phi^{-1}\tanh\phi \tag{9}$$

$$\phi = (N_L - 1)[3\rho_b/2(\rho_t - \rho_b)](3\tau\gamma_t)^{1/2} \tag{10}$$

where τ is the tortuosity factor. The nonlinear least-squares fit was calculated by allowing both γ_t and τ to vary according to eqs 7, 9, and 10; and γ_w as a function of $N_L(h)$ was obtained. A functional relationship between N_L and h was determined on the basis of SEM micrographs such as Figure 2 (bottom). The result is shown in Figure 6. The solid line in Figure 6 is a least-squares fit to the experimental data and the fitted result was used in this model. The true uptake coefficient, γ_t, and τ were determined from the nonlinear least-squares fit to be 6.3×10^{-5} and 2.18, respectively. Figure 5 also illustrates the effect of the tortuosity factor on the profile of γ_w. The curves were calculated at constant τ (=1−6). This analysis suggests that a set of curves

TABLE 2: Uptake of HOBr on NaBr Films[a]

RH%	T (K)	v (m·s^{-1})	k_s (s^{-1})	k_w (s^{-1})	γ_w	γ_t[b]
0.53 ± 0.04	250.1 ± 0.3	10.1	237 ± 24	307 ± 36	0.029 ± 0.004	3.1×10^{-3}
0.72 ± 0.06	250.3 ± 0.2	9.5	208 ± 26	265 ± 39	0.025 ± 0.004	2.4×10^{-3}
2.7 ± 0.2	250.1 ± 0.2	10.0	223 ± 22	285 ± 29	0.027 ± 0.004	2.7×10^{-3}
4.3 ± 0.3	250.3 ± 0.2	10.0	223 ± 53	288 ± 81	0.027 ± 0.008	2.7×10^{-3}
7.4 ± 0.7	250.2 ± 0.2	8.8	177 ± 42	224 ± 65	0.021 ± 0.006	1.8×10^{-3}
9.7 ± 0.8	250.4 ± 0.2	9.3	227 ± 32	292 ± 49	0.028 ± 0.005	2.9×10^{-3}
11.5 ± 1.1	250.4 ± 0.2	8.4	172 ± 23	218 ± 37	0.020 ± 0.003	1.6×10^{-3}
12.2 ± 1.9	250.0 ± 0.2	7.2	169 ± 18	221 ± 24	0.021 ± 0.004	1.8×10^{-3}
0.11 ± 0.04	260.1 ± 0.5	10.3	167 ± 74	206 ± 110	0.019 ± 0.009	1.5×10^{-3}
1.2 ± 0.2	260.1 ± 0.2	11.1	198 ± 61	245 ± 88	0.022 ± 0.008	1.9×10^{-3}
2.1 ± 0.3	259.9 ± 0.7	10.1	153 ± 28	180 ± 35	0.017 ± 0.003	1.2×10^{-3}
2.8 ± 0.3	260.1 ± 0.3	10.4	239 ± 26	309 ± 43	0.028 ± 0.004	2.9×10^{-3}
4.1 ± 0.4	260.0 ± 0.3	9.9	160 ± 55	195 ± 80	0.018 ± 0.007	1.4×10^{-3}

[a] $P_{HOBr} = (1.0 \pm 0.3) \times 10^{-6}$ Torr, $P_{total} = 0.500 \pm 0.002$ Torr, thickness = (15 ± 2) μm. [b] $N_L = 12$ and $\tau = 2.0$ were used in the HCP model calculation.

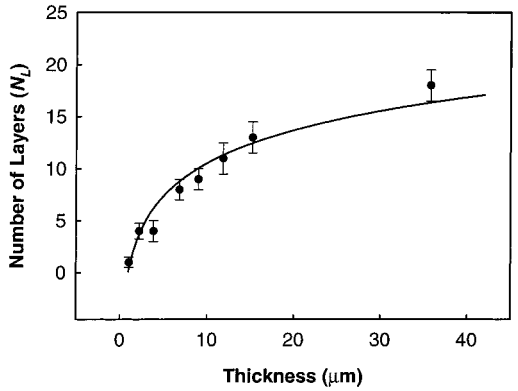

Figure 6. Plot of number of layers N_L versus the NaCl particle film thickness h. The solid line was fitted to an empirical correlation $N_L = a\log(h + b)$, where $a = 10.5217$ and $b = 0.044$.

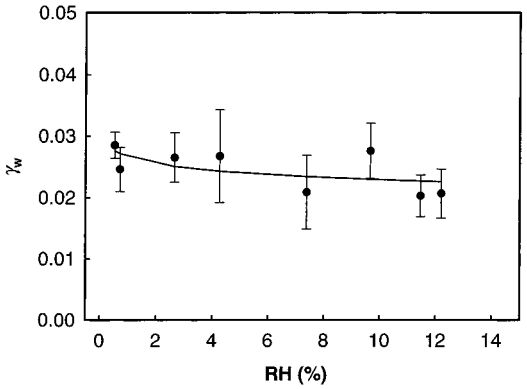

Figure 7. Plot of the initial uptake coefficient as a function of RH for HOBr on NaBr particle surfaces at 250 K. The solid line is a fit to the model as described in the text. Errors are one standard deviation of the average of a number of determinations.

with $\tau = 1-4$ can reasonably represent the experimental result, and the overall shape of the curve is not very sensitive to τ in the range of 1−4. Mochida et al. adopted $\tau = 2$ for NaCl powder and sprayed film surfaces.[18] Their adopted value is very close to our best fit. The pore-diffusion model was adopted to correct all γ_w listed in Table 1 to obtain true uptake coefficient γ_t using $\tau = 2.18$.

Uptake of HOBr on NaBr Films. A typical plot for HOBr loss on an NaBr spray-deposited film is shown in Figure 1. A product, Br_2, was observed and is plotted on the right-hand axis of the figure. However, no net Br_2 signal increase was observed when HOBr was flowed through the reactor without NaBr. The pseudo-first-order wall-loss rate constant k_s was determined to 186 s^{-1}. The diffusion-corrected first-order rate constant k_w was 232 s^{-1}, and $\gamma_w = 2.2 \times 10^{-2}$. k_s was also determined from the formation of the Br_2 signal to be 194 s^{-1}. Both results are in very good agreement.

The initial uptake coefficient of HOBr on NaBr film was studied as a function of RH at 250 and 260 K. Figure 7 shows a tendency that γ_w decreases slightly from 0.029 ± 0.004 to 0.021 ± 0.004 as RH increases from 0.53 to 12.2%. Since the decrease in γ_w is faintly larger than the uncertainty of the measurement (a typical $\pm\sigma = 0.004$, see Figure 7), the effect of RH on γ_w is very small over this RH range. γ_w of HOBr on NaBr is a factor of 10−15 higher than that on the NaCl film. This experiment was conducted at a total pressure of 0.5 Torr. This restricts the water pressure allowed in the reactor or the range of RH can be used for the experiments. However, it reduces the gas-phase diffusion correction on k_s, and a higher-accuracy γ_w value can be obtained under the fast-flow condition. The results measured at 250 and 260 K are tabulated in Table 2 along with the detailed experimental conditions. Errors are one standard deviation of the average of a number of determinations. Systematic errors in RH and T were included. γ_w values measured at 260 K are slightly lower than that of 250 K. The difference in γ_w between 250 and 260 K is small, but the difference is beyond the error of the measurements. γ_w was corrected for the surface porosity using the HCP pore-diffusion model (eq 8). It is not feasible to vary spray-deposited NaBr film thickness in a wide range to extract surface morphology information in this experiment. SEM micrographs showed that NaBr particle films were porous. We adopted $\tau = 2$ in the calculation. As we have shown previously (Figure 5) and by Keyser et al.,[41] the error in γ_t caused by τ is estimated to be less than 10%. γ_t was calculated from the mean value of γ_w directly using eqs 8−10.

Surface Deactivation. Figure 8 shows that γ of HOBr on the NaBr surface decreases as the number of repeated experiments increases. The initial uptake coefficient is 0.022, and the subsequent measurements yield $\gamma = 0.019$, 0.014, and 0.010. γ decreases about 14% after the first uptake determination and that is about 10 min in real time. This indicates that the uptake coefficient of HOBr on NaBr decreases with the increase of the surface exposure, and it is a clear indication of surface deactivation. A similar pattern was found for NaCl surfaces: the initial uptake coefficient is 1.6×10^{-3}, and the subsequent determinations of γ are 1.1×10^{-3} and 5.1×10^{-4}. These observations suggest that both active NaBr and NaCl surface sites could be either saturated with HOBr or sites are deactivated by the formation of NaOH, a product of the reaction (see Discussion).

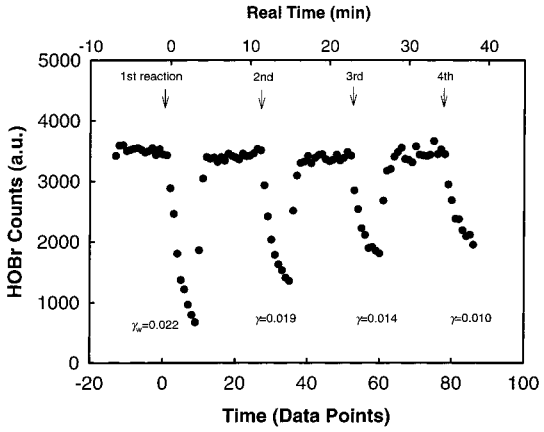

Figure 8. HOBr uptake on a spray-deposited NaBr film is shown as repeated measurements at 250.3 K, $P_{HOBr} = 1.5 \times 10^{-6}$ Torr, RH = 0.75%, and total pressure of 0.50 Torr. The arrows indicate the reference position z_0 of each determination. The initial uptake coefficient γ_w is 0.022, and subsequent γ are 0.019, 0.014, and 0.010, respectively. The result suggests that the NaBr surface becomes saturated as HOBr exposure increases. The real time of the experiment is shown on the top axis of the plot.

IV. Discussion

Uptake. We have shown that the NaX surface sites can be deactivated upon the reaction with HOBr. The surface deactivation is attributed to either HOBr adsorbing on an active surface site or a product, NaOH, consuming a site. Figure 8 demonstrates that γ decreases ~14% after the NaBr surface was taken up by HOBr in the γ_w determination. In the subsequent determinations, γ was even lower. Mochida et al. observed a similar but stronger trend of decreasing uptake coefficient with exposure to HOBr on KBr spray-deposited surfaces.[18] They also showed that the initial uptake coefficient of HOBr on NaCl and KBr decreased as [HOBr] increased, for [HOBr] less than 2×10^{10} molecules/cm^3. However, the decrease in the initial uptake coefficient was insignificant when [HOBr] was $>2 \times 10^{10}$ molecules/cm^3. This also suggests that surfaces can be saturated with HOBr.

A typical measurement error in γ_w is ~15% or higher (see Tables 1 and 2). A possible source of error includes some degree of irreproducibility of particle surfaces from experiment to experiment, the surface deactivation, and the HOBr signal fluctuation (random error). To minimize the surface deactivation effect, the following procedures were implemented during this study: (1) a shorter data acquisition time (~3 min in the real time to determine γ_w, cf. Figure 1); (2) freshly prepared NaX surfaces; and (3) lower [HOBr] (~10^{-6} Torr). The error analysis suggests that the effect of the surface deactivation on γ_w is reduced to a level that is comparable to the other random errors of the measurement.

γ_w was not measured as a function of [HOBr] because of a limitation in adjusting both [HOBr] and RH over a wide range of values. However, on the basis of the work by Mochida et al. and the results from this study, we expect that γ_w would vary slightly under the range of [HOBr] employed in this study.

Figure 1 shows the HOBr uptake remains first order for ~10 ms. However, the Br_2 release curves off at ~8 ms. A possible explanation is that some active NaBr surface sites were adsorbed by the product toward the end of the measurement and these sites were deactivated. Thus, the formation of Br_2 appears to be lower and shows the tread of curve off at 8 ms. Nevertheless, gas-phase HOBr molecules may have other loss pathways, as will be discussed later. It remains the first-order loss of almost 10 ms.

The surface morphology of the NaX particle films was taken into consideration. We found that the surface morphology of particle films, and the shapes and sizes of the salt granules, depended on the methods of preparation. NaCl granules had irregular shapes (Figure 2), and the rounded edges of granules suggest that the surface layer of the granules was wet. However, when NaCl particle films were prepared from saturated NaCl−CH_3OH solutions, the granules showed a cubic crystal-like shape. The films remained porous with internal surface areas.

The use of the pore-diffusion model to correct for internal surface areas of the particle films is an approximation. Figure 2 shows granules of salt particles are not perfect spheres as assumed in the model. The packing is not exactly SCP either. However, the model did very well in reproducing the thickness dependence on γ_w (Figure 6). This suggests that the treatment is acceptable provided that one can validate the method as illustrated in Figure 6.

Water on NaCl and NaBr Surfaces. Water molecules are known to be adsorbed on both NaCl and NaBr surfaces.[44,45] Adsorption of water on NaCl surfaces under ambient conditions has been extensively studied.[25−27,46−49] Ewing and co-workers found that adsorption of water on the NaCl(100) surface at low humidity (RH < 30%) was submonolayer and started to form "islands" and multilayer coverage at higher humidity. At multilayer coverage, there was three-dimensional growth on the surface with a low concentration of ions from the substrate being incorporated into the multilayer. At midcoverage, there was a transition between two-dimensional and three-dimensional growth.

The deliquescence point (DP) is 80 ± 4% RH at 253 K for NaCl.[50] The phase diagram of NaCl−H_2O indicates that the eutectic temperature of NaCl·2H_2O-ice-liquid is 252 K.[51−53] At low RH (RH < 22%) and 250−260 K, metastable liquid phase should not be formed in the region of interest in this study, and the bulk composition of the solid phase is mainly NaCl as suggested in the phase diagram.[52] The eutectic temperature for ice/NaBr·5H_2O is ~245 K.[52] Similarly, metastable liquid is not expected to form in a phase region with RH < 12%, as we assume that the phase diagram of NaBr/H_2O is similar to that of NaCl/H_2O at 250 K. This suggests that the reactions of HOBr with NaCl and NaBr surfaces resemble the gas−surface reactions at low RH.

Hemminger, Finlayson-Pitts, and co-workers showed that when gaseous HNO_3 molecules adsorbed on the NaCl(100) surface, a metastable nitrate film was initially formed.[54,55] Water vapor (<75% RH, below the DP of $NaNO_3$, 74.3%[55]) was then deposited on the film, the ionic mobility of metastable $NaNO_3$ increased, and deliquescence-like behavior occurred over the NaCl surface. This resulted in a quasi-liquid layer in which the $NaNO_3$ ion mobility was substantially enhanced. The precipitation of stable $NaNO_3$ finally occurred below DP.

A similar process may occur for the HOBr uptake on NaCl surfaces. After HOBr is adsorbed on NaCl, it reacts with NaCl to form NaOH and BrCl. NaOH is adsorbed on NaCl surfaces, but crystallization is thermodynamically unfavored. The adsorbed water increases the ionic mobility of NaOH and transfers NaOH into stable thermodynamic states and regenerates active Cl^- sites. This is a driving force for the reaction to be maintained. The DP of bulk NaOH is ~7%.[55] We do not expect the precipitation of NaOH crystals; rather, NaOH is in a deliquescence-like state on the surface under most experimental conditions. The rate-limiting step is expected to be the reaction between HOBr(ad) and Cl^- in which water may not play a direct role. This qualitatively explains the weak dependence of γ_w on

RH over the RH range of 1−18% (Figures 4 and 7). A quantitative discussion will be presented below.

Mechanism. The experimental observations for the HOBr reaction with the water-adsorbed NaCl solid salt are consistent with the reaction occurring in the following steps: (1) water vapor is in adsorption equilibrium with the NaCl surface; (2) HOBr reacts with Cl^- to form BrCl while H_2O is adsorbed on the surface; (3) either product or HOBr consumes active NaCl sites; (4) at a higher water coverage, ions from NaCl crystal are incorporated into three-dimensional water multilayer,[26,27,47] and HOBr can react with Cl^- over the adlayer. These processes can be expressed by the following reactions:

$$H_2O(g) + NaCl(s) \leftrightarrow H_2O(ad) \quad (11)$$

$$HOBr(g) \leftrightarrow HOBr(p) \quad (12)$$

$$HOBr(p) + S \leftrightarrow HOBr(ad) \quad (13)$$

$$HOBr(ad) + Cl^-(s) \leftrightarrow HO\cdots Br\cdots Cl(ad) \xrightarrow{k} BrCl(g) + OH^-(ad) \quad (14)$$

$$HOBr(p) + H_2O(ad) \xrightarrow{k'} HOBr(ad) \quad (14')$$

$$HOBr(ad) + Cl^-/H_2O(s) \xrightarrow{k''} BrCl(g) + OH^-(ad) \quad (14'')$$

Reaction 11 represents the water adsorption equilibrium, and the surface is ionic polycrystalline NaCl. NaCl(s) should be taken as Na^+ and Cl^- ions. HOBr is assumed to be trapped in a precursor state (reaction 12) before it migrates over the surface and reacts with Cl^- ions as on the ice surface.[36] Cl^-(s) can be from both NaCl surfaces and in H_2O multilayer. The observed HOBr loss rate can be expressed as

$$d[HOBr]/dt = \{k[HOBr(ad)](1-\theta) + k'[HOBr(p)]\theta + k''[HOBr(ad)]f\theta\}A/V \quad (15)$$

where θ is the water surface coverage, f is a fraction of multilayer islands on the water adlayer, and A/V is the surface-to-volume ratio of the reactor. The first term in eq 15 describes the reaction of HOBr with Cl^- on NaCl surface sites (reaction 14), which are not adsorbed by water; the second term is the loss of HOBr on adsorbed H_2O (reaction 14′); and the last term is the reaction of HOBr with Cl^- over multilayer water islands (reaction 14″). At RH < 25%, the water coverage is in the range of submonolayer to monolayer and $f \approx 0$.[26,46,49] The uptake coefficient of HOBr on adsorbed H_2O at 250 K is expected to be $\sim 10^{-4}$ or less. This is because the initial uptake coefficients of HOBr on the ice surface are 1.2×10^{-3} and 5.8×10^{-4} at 229 and 239 K, respectively.[36] Thus, it is expected that $k'[HOBr(p)]\theta < k[HOBr(ad)](1-\theta)$, after taking into consideration the fraction of adsorbed H_2O on the surface and the HOBr uptake coefficient on ice. This implies that the reaction occurs predominately on those sites without water adsorption, but those sites next to adsorbed water, defects, and steps are favored. As a first-order approximation, we can rewrite eq 15 as (i.e., reaction 14 only)

$$\text{rate} \approx k[HOBr(ad)](1-\theta)(A/V) \quad (16)$$

A rate expression can be derived using the steady-state approximation and total available NaCl surface site $S_o = S + [HOBr(ad)] + [OH(ad)] \approx S + 2[HOBr(ad)]$, where S_o = total NaCl sites − water adsorbed NaCl sites and S is the available reactive Cl^- site:

$$\text{rate} = kK_1K_2\frac{S_oP_{HOBr}}{1+2K_1K_2P_{HOBr}}(1-\theta)\frac{A}{V} \quad (17)$$

where $K_1 = k_{12}/k_{-12}$ and $K_2 = k_{13}/k_{-13}$. The uptake coefficient $\gamma = \frac{4\ \text{rate}}{\omega[HOBr]}\frac{V}{A}$ can be written as

$$\gamma = kK_1K_2\frac{S_o(1-\theta)}{1+2K_1K_2P_{HOBr}}\frac{4RT}{\omega L} = kK_1K_2\frac{S_o(1-C\ln cP_{H_2O})}{1+2K_1K_2P_{HOBr}}\frac{4RT}{\omega L} \quad (18)$$

where the Temkin isotherm was used to determine θ. c and C are constants used in the Temkin isotherm and L is the Avogadro constant. The Temkin isotherm describes many adsorption systems in the coverage of $0.2 < \theta < 0.8$.[56] Some constants in eq 18 can be combined (P_{HOBr} is approximately a constant in this study) and the equation $\gamma = a(1 - d\log(bP_{H_2O}))$ was used to fit uptake coefficients of HOBr on NaCl and NaBr at constant temperature and [HOBr] conditions; we assume that both mechanisms are the same. The results are plotted as solid lines in Figures 4 and 7. Overall, the fitted curves represent the experimental results well. This is a good indication that the proposed mechanism represents a correct reaction pathway at low RH (<18%) region. The uptake coefficient of HOBr on NaCl surfaces in Figure 4 appears to show a tendency of a slight increase in γ_w at RH > 18%. Equation 18 ignored the reaction of HOBr with Cl^- over the water multilayer (reaction 14″). If we take this factor into consideration, the rate expression includes a term proportional to $\theta \cdot f$. Qualitatively, this predicts that γ increases with P_{H_2O} or RH at higher humidity. In addition, the loss of HOBr to OH^- is completely ignored in eq 15, since the amount of OH^- or NaOH formed is low initially in the time period over which the initial uptake coefficient was determined. However, at a region where water coverage is either monolayer or multilayer (RH ∼ 30%), a deliquescence-like NaOH layer may cover some parts of the NaCl surface. In basic solutions, a disproportion reaction can take place.[57]

$$HOBr + OH^- \rightarrow H_2O + OBr^- \quad (19)$$

$$3OBr^- \rightarrow 2Br^- + BrO_3^- \quad (20)$$

This channel creates an additional HOBr loss and the observed initial uptake coefficient could increase at higher RH. Mössigner and Cox showed the uptake of HOI on NaOH is higher than 0.1 at RH = 11% and 278 K.[58]

Equation 18 shows that the uptake coefficient is inversely proportional to P_{HOBr}. This explains the uptake coefficient decreases with the increase in P_{HOBr} as observed by Mochida et al.[18] The observations in Figure 8 can be explained: Subsequent increase in HOBr exposure to the surface resulted in the adsorption of OH^-(ad) and HOBr(ad) on the surface; this reduces the amount of available reactive Cl^- sites, S, on the surface. A surface deactivation was observed in the experiment.

The adsorption of water on NaBr surfaces is similar to that on NaCl surfaces. The shape of water isotherms on both surfaces at $P/P_o < 0.2$ is nearly the same,[44,45] and thus predicted profiles of the uptake coefficient based on eq 18 fit the results of HOBr on both NaCl and NaBr very well. The ionic nature of the reaction (cf. eq 14) is expected on the basis of reactions HOBr

with HCl and HBr;[36,59] therefore, the mechanism outlined above applies to both cases, as was demonstrated in Figures 4 and 7. The conclusion of this discussion is the following: Under conditions of low RH (RH < 18%), the reaction takes place predominately on NaCl surface sites without water adsorption. The water coverage, θ, does not dramatically change with RH, suggesting active surface sites are regenerated as OH^-(ad) is converted to the deliquescence-like state on the surface. The role of water or RH is that it increases the ion mobility of NaOH over the surface and provides a lower energy pathway for NaOH to form a stable deliquescence-like state. The weak dependence of γ_w on RH also suggests that water may not play a direct role in the rate-limiting step (reaction 14).

Comparison with Previous Studies. The uptake of HOBr on NaCl and KBr was measured in the Knudsen reactor at very low humidity conditions <1% and on deliquescent NaCl aerosols (75% RH) and in frozen and aqueous salt solutions.[18,19,21,59] Although we may compare some of our results with these studies, a direct comparison for γ as a function of RH is not feasible.

Mochida et al. reported that the initial uptake coefficient of HOBr on powder and grain NaCl was from 65 to 6.5×10^{-4} at 2×10^{13} to 6×10^{14} molecules/s ($\sim 10^9 - 10^{10}$ molecules/cm^3) at room temperature.[18] This initial uptake coefficient was corrected to be equivalent to the initial uptake coefficient obtained from a spray-deposited thin NaCl particle film, which was assumed to be no internal surface areas. Spray-deposited NaCl substrates could not be used for measuring the uptake coefficient of HOBr because the HOBr signal change before and after the reaction was too small. This initial uptake coefficient is estimated to be $\sim 10^{-4}$ under our experimental conditions. At RH = 1.5−1.9%, we obtained $\gamma_w = 1.5-2.0 \times 10^{-3}$ at 250 K (Figure 4), and the true uptake coefficient γ_t is 6.3×10^{-5}. γ_t is estimated to be a factor of ~10 lower than the initial uptake coefficient reported by Mochida et al. The NaCl substrates used by Mochida et al. were ground in a ball mill, with average diameters between 10 and 100 μm or 350−500 μm. Similar to our treatment, the internal surface areas were corrected using the pore-diffusion model developed by Keyser et al.[41,42] However, surface reactivity of ground salt samples may be different from that of aerosol-deposited substrates in terms of surface defects and steps. Our sample involved recrytallization from liquid aerosols to solid particles on the detachable glass tube surface at 150 °C. The recrystallization may create internal surfaces (Figure 2), but the annealing at high temperature may reduce the defects or steps on the granule surface. This may explain why the uptake coefficient γ_t is lower than the one reported by Mochida et al.

Abbatt and Waschewsky reported an upper limit to the uptake coefficient of HOBr on unbuffered deliquescent NaCl aerosols (75% RH) to be 1.5×10^{-3} at 298 K and [HOBr] = $10^{12}-10^{13}$ molecules/cm^3.[21] In acidified aerosols, γ was 0.5. As their experimental conditions were very different from those of the current study in terms of both RH (liquid versus solid) and [HOBr], a quantitative comparison cannot be made. However, γ measured in unbuffered aerosols is comparable with γ_w and it is higher than γ_t. Combined with the results of our study, this suggests that the effect of RH (1−75%) on the initial uptake coefficient is not very large. The formation of BrCl was observed both on NaCl powder surfaces and in aqueous salt solutions.[18,19]

There is no reported study on the uptake of HOBr on NaBr surfaces. Kirchner et al. studied the HOBr uptake in frozen NaBr solutions.[59] The closest system to compare is the HOBr uptake on KBr spray-deposited surfaces.[18] The γ was $2-6 \times 10^{-2}$ at [HOBr] = 10^{10} molecules/cm^3 and room temperature. Mochida et al.[18] also reported that addition of water vapor ($10^{-4}-10^{-3}$ Torr, RH < 1%) did not have an effect on γ. Our study was conducted at 250 and 260 K and RH = 0.5−12.2%; we found γ_w has a tendency to be slightly lower at higher T. γ_w (=0.029 ± 0.04 at RH = 0.53%) is within the ranges of γ. Kirchner et al. reported a γ value of 3.3×10^{-3} on 30% NaBr frozen solution at 230−240 K.[59] We may assume the surface of frozen solutions is smooth; γ_t is used to compare with the result of Kirchner et al. With $\gamma_t = 1.8 \times 10^{-3}$ at our highest RH = 12.2 and 250 K, it is numerically in good agreement with the result of Kirchner et al. despite the differences in the nature of the surface.

Atmospheric Implications. Sea-salt particles exist in the marine boundary layer and in the lower stratosphere after volcanic eruption. Salt particles most often occur as deliquescent aerosols in the marine boundary layer. However, some of these particles may be transported to a dry atmosphere where they are found as solid crystalline salt particles.[60] The purpose of this study was to examine the heterogeneous activation of Br and Cl species and the role of adsorbed water on NaX. The critical question is whether heterogeneous activation of HOBr via the reactions of HOBr + NaCl and HOBr + NaBr is competitive with photolysis of HOBr to active Br (and Cl) species.

The photolysis rate constant J for HOBr → OH + Br is $\sim 10^{-3}$ s^{-1} at ground level.[61] The photochemical lifetime of HOBr is approximately 1 h. The photochemical lifetimes of Br_2 and BrCl are 1 and 3 min, respectively, on the basis of photolysis rates of Br_2, $J = 2 \times 10^{-2}$, and BrCl, $J = 6 \times 10^{-3}$ s^{-1}.[15,62] The importance of reactions 2 and 3 is that two halogen atoms are released into the gas phase per HOBr consumed, thus increasing the halogen atom concentration in the troposphere by converting photochemical inactive sea salt and temporally reservoir HOBr. Heterogeneous loss lifetime t_τ of HOBr on NaX can be estimated as

$$t_\tau = 4/(\omega \gamma_t A_c) \qquad (21)$$

where A_c is a condensed surface-to-air volume ratio (cm^2/cm^3). When we assume a sea-salt aerosol loading of 4×10^{-6} cm^2/cm^3, corresponding to approximately 10 particles/cm^3 with a particle radius of 10^{-4} cm,[63] lifetimes of ~4.5 h and ~9 days are estimated for HOBr on the NaBr and NaCl aerosol surface using $\gamma_t = 2.5 \times 10^{-3}$ and 5×10^{-5}, respectively. There are other factors such as morphology of aerosols that affect the lifetime calculation, but they are omitted in this estimation. The lifetime calculation suggests that bromine activation via reaction 2 is probably competitive with photolysis of HOBr in the troposphere, whereas reaction 3 is approximately 2 orders of magnitude slower than photolysis under dry sea-salt aerosol-loading conditions. However, with a higher γ value on an acidic deliquescent NaCl aerosol,[21] the heterogeneous activation of HOBr over NaCl aerosols would be favored over photolysis in Br and Cl activation. On the other hand, we have shown that sea-salt surfaces can be deactivated slowly when it reacts with HOBr; if all active sea-salt aerosol surfaces were consumed, heterogeneous reactions 2 and 3 play little role in halogen activation. A surface regeneration process would be required for nondeliquescent aerosols to play a major role in the atmosphere. The surface regeneration can be achieved by adsorbed water as has been discussed previously or by continued supplies of aerosols in the boundary layer. Future studies are required to assess surface regeneration processes.

Conclusions

We have for the first time determined the uptake of HOBr on NaCl and NaBr particle films as a function of RH. The initial

uptake coefficient γ_w of HOBr on NaCl surfaces decreases slightly from $2.0 \pm 0.3 \times 10^{-3}$ to $8.1 \pm 1.3 \times 10^{-4}$ as RH increases from 1.5 to 18.2% at 250 K. γ_w increases sharply as the NaCl film thickness increases from 1 to 50 μm and then levels out gradually. The γ_w value of HOBr on NaBr showed a weak decreasing tendency from 0.029 ± 0.004 to 0.021 ± 0.004 at 250 K as RH increases from 0.53 to 12.2%. The tendency is small, but it is outside the error of the measurement. The granule size distribution of the NaCl particle film was studied using SEM, and the tortuosity factor, τ, was 2.18. The true uptake coefficients γ_t were calculated using the pore-diffusion model. γ_t of HOBr on NaCl also showed a decrease from 6.6×10^{-5} to 2.6×10^{-5} as RH increases from 1.5 to 18.2% at 250 K. A weak decreasing tendency in γ_t from 3.1×10^{-3} to 1.6×10^{-3} at 250 K was observed for HOBr on NaBr as RH increases from 0.53 to 12.2%. The mechanism for HOBr + NaCl $\rightarrow$ BrCl + NaOH and HOBr + NaBr $\rightarrow$ Br_2 + NaOH involves a step for HOBr interaction with X^- on the surface. We have shown that the reactions occur predominantly on a NaX surface where no water is adsorbed at the condition of low RH. Adsorbed water could enhance the ion mobility of NaOH on salt surfaces, and the weak dependence of γ_w on RH suggests water may not play a direct role in the rate-limiting step (reaction 14). The heterogeneous reaction rate of HOBr + NaBr $\rightarrow$ Br_2 + NaOH is competitive with HOBr photolysis rate at the boundary layer.

Acknowledgment. The authors acknowledge discussions with Professors Barbara Finlayson-Pitts, George Ewing, and Scot Martin. We also thank Dr. W. Samsonoff for assistance in obtaining SEM micrographs of salt samples at the Wadsworth Center's Electron Microscopic Core Facility and Dr. Oliver Rattigan and two anonymous reviewers for helpful suggestions and comments on the manuscript. This work was supported by the Atmospheric Chemistry Program, National Science Foundation.

References and Notes

(1) Barrie, L. A.; Bottenheim, J. W.; Schnell, R. C.; Crutzen, P. J.; Rasmussen, R. A. *Nature* **1988**, *334*, 138.
(2) McConnell, J. C.; Henderson, G. S.; Barrie, L. A.; Bottenheim, J.; Niki, H.; Langford, C. H.; Templeton, E. M. J. *Nature* **1992**, *355*, 150.
(3) Fan, S. M.; Jacob, D. J. *Nature* **1992**, *359*, 522.
(4) Tang, T.; McConnell, J. C. *Geophys. Res. Lett.* **1996**, *23*, 2633.
(5) Impey, G. A.; Shepson, P. B.; Hastie, D. R.; Barrie, L. A.; Anlauf, K. G. *J. Geophys. Res.* **1997**, *102*, 16005.
(6) Hebestreit, K.; Stutz, J.; Rosen, D.; Matveev, V.; Peleg, M.; Luria, M.; Platt, U. *Science* **1999**, *283*, 55.
(7) Finlayson-Pitts, B. J.; Livingston, F. E.; Berko, H. N. *Nature* **1990**, *343*, 622.
(8) Behnke, W.; Krüger, H.-U.; Scheer, V.; Zetzsch, C. *J. Aerosol Sci.* **1991**, *22*, S609.
(9) Vogt, R.; Finlayson-Pitts, B. J. *J. Phys. Chem.* **1994**, *98*, 3747.
(10) Fenter, F. F.; Caloz, F.; Rossi, M. J. *J. Phys. Chem.* **1996**, *100*, 1008.
(11) Davis, J. A.; Cox, R. A. *J. Phys. Chem. A* **1998**, *102*, 7631.
(12) Ghosal, S.; Hemminger, J. C. *J. Phys. Chem. A* **1999**, *103*, 4777.
(13) Gershenzon, M. Y.; Il'In, S.; Fedotov, N. G.; Gershenzon, Y. M. *J. Atmos. Chem.* **1999**, *34*, 119.
(14) Weis, D. D.; Ewing, G. E. *J. Phys. Chem. A* **1999**, *103*, 4865.
(15) Sander, R.; Crutzen, P. J. *J. Geophys. Res.* **1996**, *101*, 9121.
(16) Timonen, R. S.; Chu, L. T.; Leu, M.-T.; Keyser, L. F. *J. Phys. Chem.* **1994**, *98*, 9509.
(17) Caloz, F.; Fenter, F. F.; Rossi, M. J. *J. Phys. Chem.* **1996**, *100*, 7494.
(18) Mochida, M.; Akimoto, H.; van den Bergh, H.; Rossi, M. J. *J. Phys. Chem. A* **1998**, *102*, 4819.
(19) Fickert, S.; Adams, J. W.; Crowley, J. N. *J. Geophys. Res.* **1999**, *104*, 23719.
(20) Gebel, M.; Finlayson-Pitts, B. J. *J. Phys. Chem. A* **2001**, *105*, 5178.
(21) Abbatt, J. P. D.; Waschewsky, G. C. G. *J. Phys. Chem. A* **1998**, *102*, 3719.
(22) Vogt, R.; Crutzen, P. J.; Sander, R. *Nature* **1996**, *383*, 327.
(23) Mozurkewich, M. *J. Geophys. Res.* **1995**, *100*, 14199.
(24) Beichert, P.; Finlayson-Pitts, B. J. *J. Phys. Chem.* **1996**, *100*, 15218.
(25) Peters, S. J.; Ewing, G. E. *Langmuir* **1997**, *26*, 6345.
(26) Foster, M. C.; Ewing, G. E. *J. Chem. Phys.* **1999**, *26*, 102.
(27) Foster, M. C.; Ewing, G. E. *J. Chem. Phys.* **2000**, *112*, 6817.
(28) Hu, J. H.; Abbatt, J. P. D. *J. Phys. Chem. A* **1997**, *101*, 871.
(29) Hallquist, M.; Stewart, D. J.; Baker, J.; Cox, R. A. *J. Phys. Chem. A* **2000**, *104*, 3984.
(30) Kane, S. M.; Caloz, F.; Leu, M.-T. *J. Phys. Chem. A* **2001**, *105*, 5465.
(31) Behnke, W.; Scheer, V.; Zetzsch, C. *J. Aerosol Sci.* **1993**, *24*, S115.
(32) George, Ch.; Ponche, J. L.; Mirabel, Ph.; Behnke, W.; Scheer, V.; Zetzsch, C. *J. Phys. Chem.* **1994**, *98*, 8780.
(33) Seinfeld, J. H.; Pandis, S. N. *Atmospheric Chemistry and Physics;* Wiley: New York, 1998; chapter 9.
(34) Chu, L. T.; Heron, J. W. *Geophys. Res. Lett.* **1995**, *22*, 3211.
(35) Chu, L.; Chu, L. T. *J. Phys. Chem. A.* **1999**, *103*, 691.
(36) Chu, L.; Chu, L. T. *J. Phys. Chem. A* **1999**, *103*, 8640.
(37) Dean, J. A. *Lange's Handbook of Chemistry*, 15th ed.; Wiley: New York, 1999; p 5.26 and 3.49.
(38) Chu, L.; Chu, L. T. *Recent Res. Devel. Geophys.* **2000**, *3*, 141.
(39) Brown, R. L. *J. Phys. Natl. Bur. Stand (U. S.).* **1978**, *83*, 1.
(40) *Perry's Chemical Engineering Handbook*; Perry, R. H., Green, D. W., Eds.; McGraw-Hill: New York, 1997; p 5.50.
(41) Keyser, L. F.; Moore, S. B.; Leu, M.-T. *J. Phys. Chem.* **1991**, *95*, 5496.
(42) Keyser, L. F.; Leu, M.-T.; Moore, S. B. *J. Phys. Chem.* **1993**, *97*, 2800.
(43) Underwood, G. M.; Li, P.; Usher, C. R.; Grassian, V. H. *J. Phys. Chem. A* **2000**, *104*, 819.
(44) Barraclough, P. B.; Hall, P. G. *Surf. Sci.* **1974**, *46*, 393.
(45) Chikazawa, M.; Kaiho, M.; Kanazawa, T. *Nippon Kagaku Kaishi* **1976**, *3*, 410.
(46) Peters, S. J.; Ewing, G. E. *J. Phys. Chem. B* **1997**, *101*, 10880.
(47) Engkvist, O.; Stone, A. J. *J. Chem. Phys.* **2000**, *112*, 6827.
(48) Luna, M.; Rieutord, F.; Melman, N. A.; Dai, Q.; Salmeron, M. *J. Phys. Chem. A* **1998**, *102*, 6793.
(49) Romakkaniemi, S.; Hämeri, K.; Väkevä, M.; Laaksonen, A. *J. Phys. Chem. A* **2001**, *105*, 8183.
(50) Cziczo, D. J.; Abbatt, J. P. D. *J. Phys. Chem. A* **2000**, *104*, 2038.
(51) *International Critical Table*; Washburn, E. W., Ed.; McGraw-Hill: New York, 1926; Vol. 1, p 63; Vol. 2, p 327.
(52) Koop, T.; Kapilashrami, A.; Molina, L. T.; Molina, M. J. *J. Geophys. Res.* **2000**, *105*, 26393.
(53) Martin, S. T. *Chem. Rev.* **2000**, *100*, 3409.
(54) Allen, H. C.; Laux, J. M.; Vogt, R.; Finlayson-Pitts, B. J.; Hemminger, J. C. *J. Phys. Chem.* **1996**, *100*, 6371.
(55) Laux, J. M.; Fister, T. F.; Finlayson-Pitts, B. J.; Hemminger, J. C. *J. Phys. Chem.* **1996**, *100*, 19891.
(56) Rudzinski, W.; Everett, D. H. *Adsorption of Gases on Heterogeneous Surfaces*; Academic Press: San Diego, CA, 1992; pp 51−53.
(57) Cotton, F. A.; Wilkinson, G. *Advanced Inorganic Chemistry*, 4th ed.; Wiley: New York, 1980; pp 558.
(58) Mössinger, J. C.; Cox. R. A. *J. Phys. Chem. A* **2001**, *105*, 5165.
(59) Kirchner, U.; Benter, Th.; Schindler, R. N. *Ber. Bunsen-Ges. Phys. Chem.* **1997**, *101*, 975.
(60) Shaw, G. E. *J. Geophys. Res.* **1991**, *96*, 22369.
(61) Rattigan, O. V.; Lary, D. J.; Jones, R. J.; Cox, R. A. *J. Geophys. Res.* **1996**, *101*, 23021.
(62) Impey, G. A.; Mihele, C. M.; Anlauf, K. G.; Barrie, L. A.; Hastie, D. R.; Shepson, P. B. *J. Atmos. Chem.* **1999**, *34*, 21.
(63) Using marine aerosol concentration of ~2000 cm^{-3} with the size of a micron (Kim, Y.; Sievering, H.; Boatman, J.; Wellman, D.; Pszenny, A. *J. Geophys. Res.* **1995**, *100*, 23027) and the ratio of $[Cl^-]/[Br^-]$ near aerosol surfaces of ~188 (Foster, K. L. et al. *Science* **2001**, *291*, 471), the bromine aerosol density is approximately equivalent to 10 cm^{-3}. This corresponds to bromine sea-salt aerosol loading of 10^{-6} cm^2/cm^3 or lower and chlorine sea-salt aerosol loading $>10^6$ cm^2/cm^3. A value of 4×10^6 cm^2/cm^3 was used to estimate the lifetime.